Z. Phys. C – Particles and Fields 44, 187–198 (1989)

Zeitschrift für Physik C Particles and Fields

A study of wrong-sign single muon production in ν_μ-nucleon interaction

S.R. Mishra, P.S. Auchincloss[1], R. Blair[2], C. Haber[3], M. Ruiz[4], E. Oltman, F.J. Sciulli, M.H. Shaevitz, W.H. Smith[5]
Columbia University, New York, NY 10027, USA

F.S. Merritt, M. Oreglia, P. Reutens[6]
University of Chicago, Chicago, Ill 60637, USA

R. Coleman, H.E. Fisk, M.J. Lamm, D. Levinthal[7], D.D. Yovanovitch, W. Marsh, P.A. Rapidis, H.B. White
Fermilab, Batavia, IL 60510, USA

A. Bodek, F. Borcherding[8], N. Giokaris[9], K. Lang[10], I.E. Stockdale[11]
University of Rochester, Rochester, NY 14627, USA

Received 15 June 1989

Abstract. We report on a search for ν_μ-induced events where the single emerging muon carries lepton number opposite that of the incident neutrino. The rate and kinematic quantities of the candidate events are compared with known backgrounds from $\bar{\nu}_\mu$-induced charged current interactions and ν-induced interactions that produce dileptons. We derive an upper limit on the rate of wrong-sign single muon production relative to the rate of ν_μ charged current interactions to be 1.6×10^{-4} for $y < 0.5$ and 3.1×10^{-4} for $y > 0.5$ (90% CL). These upper limits enable us to constrain exotic sources of wrong-sign muons such as the charm component of the nucleon sea, flavor changing neutral currents and lepton number violating processes. Finally, the rate and kinematic properties of these events are compared with those of the neutrino-induced opposite-sign dimuon events.

Introduction

We report on an experimental study of ν_μ-induced wrong-sign single muon (WSM) events. In a WSM event the charge of the muon in the final state, and hence its lepton number, is opposite to the one expected from lepton number conservation:

$$\nu_\mu + N \to \mu^+ + X,$$

where X does not contain a μ. An definite excess of WSM events over known backgrounds would indicate new physics. Furthermore, the study of WSM could shed some light on the observation of like-sign dimuon events (LSDM) in $\nu_\mu - N$ scattering experiments. Prompt LSDM signals ($\nu_\mu + N \to \mu^- + \mu^- + X$) have been reported to exist at about the two standard deviation level (2σ) by several low-energy ($E_\nu < 250$ GeV) neutrino experiments [1], and, were considered unaccountable by charm-anticharm pair creation in the hadron shower of a normal charged cur-

Present addresses:
[1] Rutgers University, Piscataway, NJ 08854, USA
[2] Argonne National Laboratory, Argonne, IL 60439, USA
[3] LBL, Berkeley, CA 94720, USA
[4] CERN, Geneva, Switzerland
[5] University of Wisconsin, Madison, WI 53706, USA
[6] SLAC, Stanford, CA 94305, USA
[7] Florida State University, Tallahassee, FL 32306, USA
[8] Fermilab, Batavia, IL 60510, USA
[9] Rockefeller University, New York, NY 10021, USA
[10] Stanford University, Stanford, CA 94305, USA
[11] University of Cincinnati, Cincinnati, OH 45221, USA

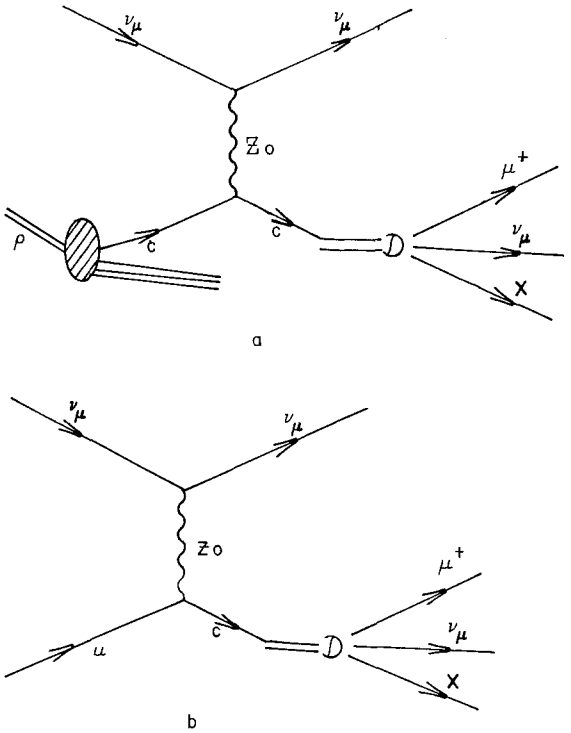

Fig. 1. a Production of a WSM from the neutral current interaction of a ν_μ with the charm quark of the nucleon sea. **b** Flavor changing NC giving rise to a WSM

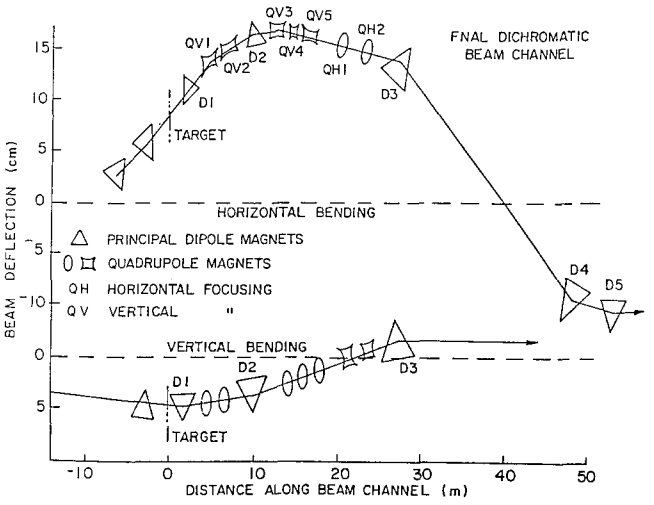

Fig. 2. Schematic diagram of the Fermilab dichromatic magnet train for the narrow band ν beam. The schematic illustrates the bending of the secondary hadron in both the horizontal and vertical views

rent (CC) interaction (the only possible source for LSDM within standard model). Since the rate of prompt WSM is comparable to that of the prompt LSDM ($\approx 10^{-4}$ per CC event), it was suggested that WSM might be the neutral current (NC) analog of some exotic mechanism giving rise to LSDM [2, 3]. The recent measurements of LSDM by the CCFR collaboration [4], however, unequivocally rules out a possible new threshold responsible for prompt LSDM. In addition to these experimental motivations, various extensions of the standard model predict the occurrence of WSM. Some interesting sources of WSM are:

(1) Charmed component of the nucleon sea: If the nucleon sea has a charmed component then ν_μ could interact with it via NC interaction: $\nu_\mu + c \to \nu_\mu + c$. The subsequent semileptonic decay of the emerging charm quark ($c \to \mu^+ + \nu_\mu + X$) would give rise to a μ^+ in the final state (see Fig. 1a).

(2) Flavor changing neutral currents [5]; if a valence up quark could be converted to a charm quark via NC interaction, then the μ^+ might come about from the prompt decay of the charm quark (see Fig. 1b): $\nu_\mu + u \to \nu_\mu + c + X$.

(3) Lepton number violation: If lepton number is not strictly conserved (via, neutrino oscillation, Majorana neutrinos etc.), ν_μ interactions could produce WSM at the lepton vertex.

The search for WSM events was made in a sample of neutrino data accumulated during two runs with the CCFR neutrino detector in the Fermilab narrow band neutrino beam (NBB). The largest background in a neutrino-induced WSM search comes from the ordinary antineutrino CC interactions. In order to improve upon the existing upper limits on the aforementioned exotic sources, the fractional $\bar{\nu}_\mu$ contamination in a ν_μ beam must be less than 10^{-3}. This crucial requirement is met by the Fermilab NBB [6]. We have performed WSM searches only in $\nu_\mu - N$ interactions. To search for WSM's in a $\bar{\nu}_\mu$ beam is intractable because ν_μ contamination is an order of magnitude higher than $\bar{\nu}_\mu$ contamination in a ν_μ beam. The first run (Fermilab experiment E 616) was conducted from June 1979 to January 1980 with an integrated proton flux (for ν_μ and $\bar{\nu}_\mu$ beams) of 5.4×10^{18}. The second run (Fermilab experiment E 701) took place in 1982 with an integrated proton flux of 3.4×10^{18} [1]. For E 701, primarily a neutrino oscillation search experiment, the fiducial volume of the neutrino detector was reduced by 34% from that of E 616.

ν-Source and the narrow band neutrino beam

A high purity of the incident ν_μ beam, with minimal $\bar{\nu}_\mu$ contamination, is crucial to the study of WSM. This was accomplished in the Fermilab NBB by (1) targeting the incident primary protons at an angle of 11.94 milliradians (mrad) in the horizontal direction and 1.13 mrad in the vertical direction with respect to the beam axis, as shown in Fig. 2; and (2) pointing the secondary hadron beam away from the

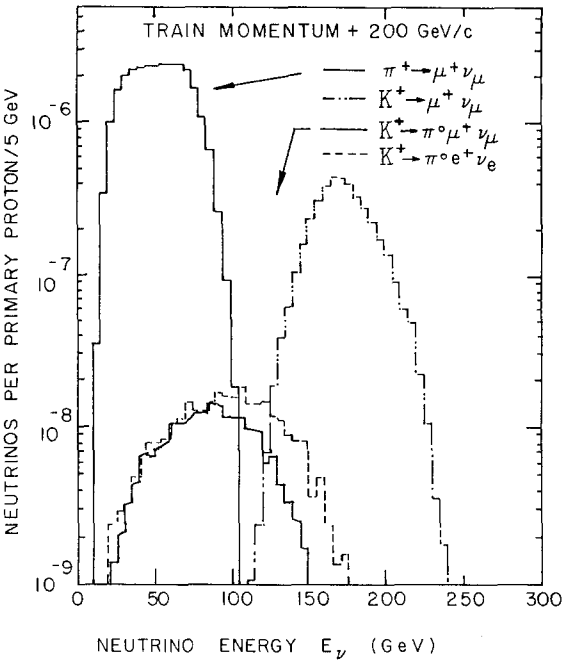

Fig. 3. Neutrino spectrum at Lab – E. The plot was simulated for 200 GeV π^+/K^+ traversing the decay pipe. The neutrinos (ν_μ and ν_e) resulted from two body and three body decays of the mesons

neutrino detector until the secondary hadrons have undergone momentum and sign selection. We will refer to ν_μ and $\bar{\nu}_\mu$ arising from π/K decay prior to momentum and sign selection as the wide band background (WBB). The simulation of WBB $\bar{\nu}_\mu$ has been outlined in Appendix A. A further reduction in the noise-to-signal ratio was achieved by the large separation (1352 m) between the primary target and the ν-detector. The WBB ν_μ and $\bar{\nu}_\mu$ flux illuminate the apparatus uniformly, whereas the sign and momentum selected NBB ν_μ's are collimated at the center of the detector. The NBB neutrinos have a characteristic energy and decay angle correlation, given by:

$$E_{\nu_\mu} = \frac{E_{\pi,K}[1-(m_\mu/m_{\pi,K})^2]}{[1+(\gamma_{\pi,K}\theta_\nu)^2]}.$$

Here $\gamma_{\pi,K} = (E/m)_{\pi,k}$, θ_ν is decay angle of the neutrino with respect to the π/K trajectory which is approximated by R/L, where R is the transverse radius of the neutrino event at the detector and L is the longitudinal distance of the interaction vertex from the point of decay of the meson. For the data presented here, $E_{\pi/K}$ equals the momentum setting of (positively charged) hadron system, with fractional momentum bite of $\pm 11\%$: 250, 200, 165, 140, 120 (E 616), or 100 (E 701 only) GeV, and produced NBB ν_μ from subsequent decays of the mesons in a 352 m evacuated decay pipe. Neutrino flux at the detector from pion decay, two-body kaon decay, and three-body kaon decay are illurstrated in Fig. 3.

The primary proton beam and the secondary beam, which consisted of π^+, K^+ and protons, were monitored at various stations along the beam transport and decay region. The total intensity of the secondary beam was measured using ionization chambers and a tuned rf cavity. A Cerenkov counter furnished the beam composition. The steering of the secondary beam was monitored using two pairs of split-plate ionization chambers. The details of the neutrino beamline, its overall design, focusing elements, and monitoring devices have been discussed by Blair et al. [7]. The total integrated proton flux for the data described in this paper was 5.55×10^{18}.

The neutrino detector

The neutrino detector [8, 9] was placed in Lab E, located 1292 m downstream of the beginning of the decay pipe. The detector is shown in Fig. 4. The detector consisted of a target calorimeter instrumented with liquid scintillation counters and spark chambers, followed by an iron toroidal muon spectrometer. The 690-ton target calorimeter was instrumented with one hundred and sixty-eight 3 m × 3 m × 5 cm steel plates, eighty-two 3 m × 3 m liquid scintillation counters, located every 10 cm of steel, and thirty-six 3 m × 3 m spark chambers with magnetostrictive readout, located every 20 cm of steel. The mean density of the target was 4.27 g/cm^3. The 310 ton muon spectrometer, also instrumented with scintillation counters and spark chambers (Fig. 4), consisted of three 3 m-long iron toroidal magnets (containing 1.6 m of steel each) with a 1.8 m outer radius and a 12.7 cm radius hole for the coils. The toroid gaps were instrumented with 1.5 m × 3 m and 3 m × 3 m spark chambers as well as the gap at the midplane of each toroid. Total transverse momentum delivered by the three toroids was 2.4 GeV/c. The detector was calibrated for hadron energy (E_{had}) and muon momentum (E_μ) measurements using a test beam of known energy. The stability of target calorimeter calibration was monitored by examining minimum ionizing muons. The *rms* hadron energy resolution was $0.89\sqrt{E_{\text{had}}(\text{GeV})}$. The *rms* muon momentum resolution was $0.11\,E_\mu$.

Analysis of WSM events

The sample of WSM events was prepared in two stages. First the events were selected from the 350000 muon triggers collected during neutrino running (when the toroid polarity was set to focus μ^-). The candidate events were required to have a defocus-

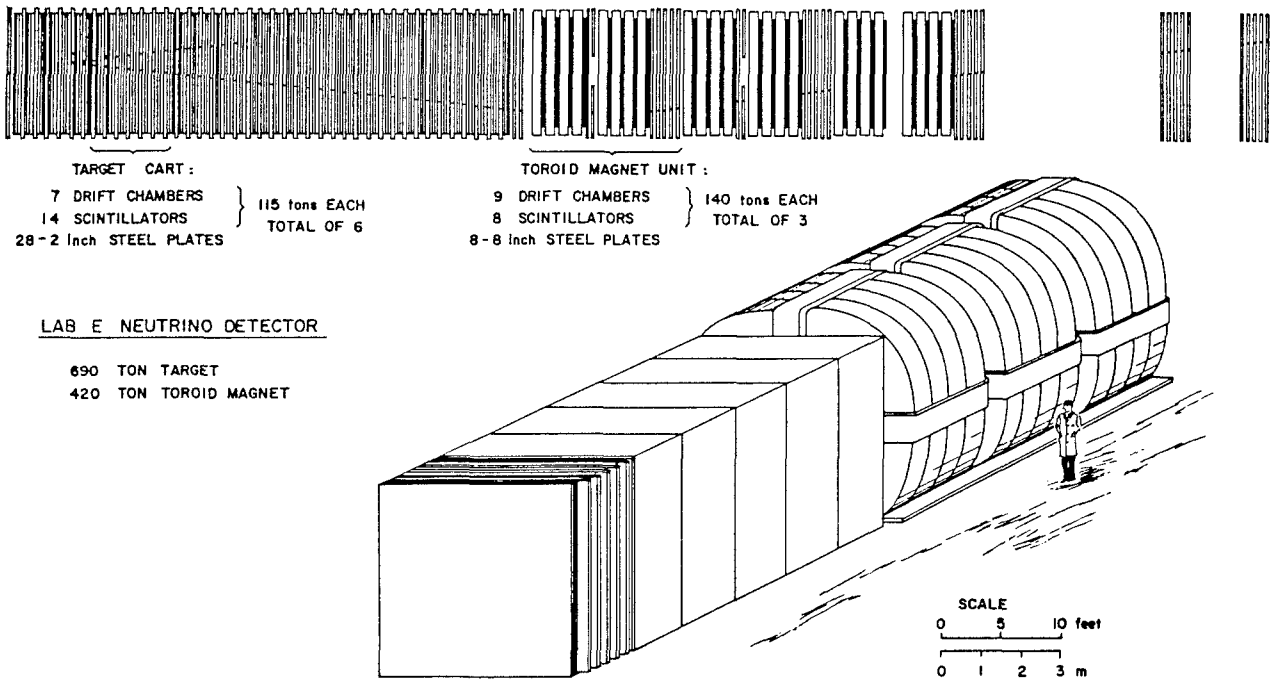

Fig. 4. The CCFR ν-detector: The 690 ton steel calorimeter target is instrumented with counters (for hadron calorimetry) and spark chambers (for muon tracking). The spectrometer, following the target, measures the muon momentum

ing muon, a transverse event vertex within a 2.7 m $\times$ 2.7 m square and a longitudinal vertex at least 3.9 m (1.9 m of iron) upstream of the front face of the spectrometer. These requirements ensured efficient measurements of the hadron and muon energies. No cut on E_{had} or the total visible energy ($E_{\text{vis}} = E_\mu + E_{\text{had}}$) was made in order to allow the comparison of the low end of the WSM energy spectrum with the WBB Monte Carlo calculation (MC). An exception was made for the small sample of slow spill data [9], where a total visible energy cut of 20 GeV was imposed to eliminate the large cosmic ray background with a candidate wrong sign track. The preliminary sample from both experiments consisted of 1600 events. The selection inefficiency for this preliminary sample of WSM was estimated to be less than 1% by scanning 30% of the total muon triggers which did not contain a clear focusing track.

For the second stage analysis all candidate WSM events were scanned on a high resolution graphics terminal. The event reconstruction of each event was examined and, where necessary ($\approx$ 15% of the events), spark chamber hits were interactively reassigned to the correct track and muon momenta were recalculated. The inefficiency of this visual scan was estimated to be well below 1% from a triple scan of the entire sample by physicists. A few additional cuts were applied to the sample. The polar angle of the defocusing muon was required to be less than 200 mrads. Of the 1600 events, the sign of the momentum could not be determined in 26 of the events. These ambiguous events, which traversed only a small part of the spectrometer, were eliminated by requiring that the radius of the projected track at the front face of the spectrometer be greater than 12.7 cm inwards from the outer edge. Finally, a cut of 7.5 GeV was imposed on the energy of the muon. With these cuts the probability that a μ^- would appear as a μ^+ was less than 6×10^{-5}. In addition to the apparatus-related cuts a beam-steering cut was imposed on a spill-by-spill basis to insure properly directed primary and secondary beams [10].

The final sample of WSM consisted of 443 events. Figures 5a, 6a and 7a display histograms (solid line) of E_{vis}, E_μ, and E_{had} for the WSM data (the cumulative Monte Carlo contributions to WSM, discussed below, are shown by dotted line). The initial rise in the total visible energy spectrum (Fig. 5a) is due to geometric and kinematic acceptance. Since WBB $\bar{\nu}_\mu$ event is expected to constitute the largest background, the data were also examined after imposing an additional requirement that the inelasticity variable, $y = E_{\text{had}}/E_{\text{vis}}$, be greater than $\frac{1}{2}$. Figure 9 shows the scatterplot of y vs. E_{vis}. One notices that data separate into two bands: low-y, low-E_ν events are predominantly $\bar{\nu}_\mu$ CC interactions and high-y, high-E_ν events are predominantly ν-interactions that produce dileptons. Here and in subsequent sections all calculations will be considered both with and without this y cut. Figures 5b, 6b and 7b illustrate E_{vis}, E_μ and E_{had} distributions of the sample with $y > 0.5$. From the dichromatic nature of the NBB the energy of the inci-

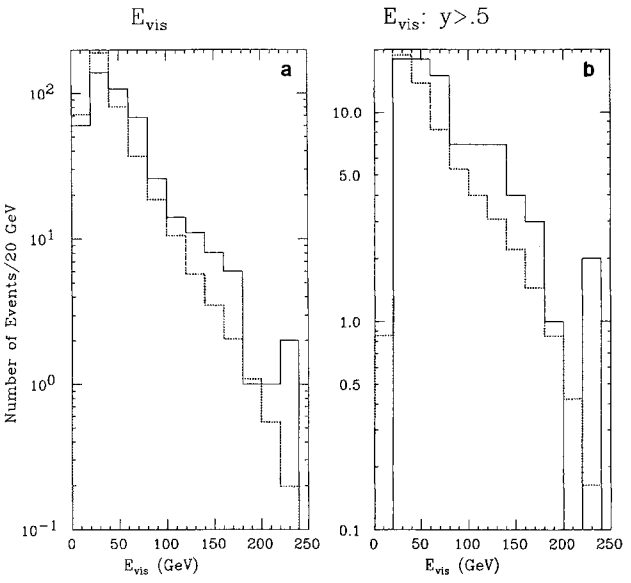

Fig. 5a, b

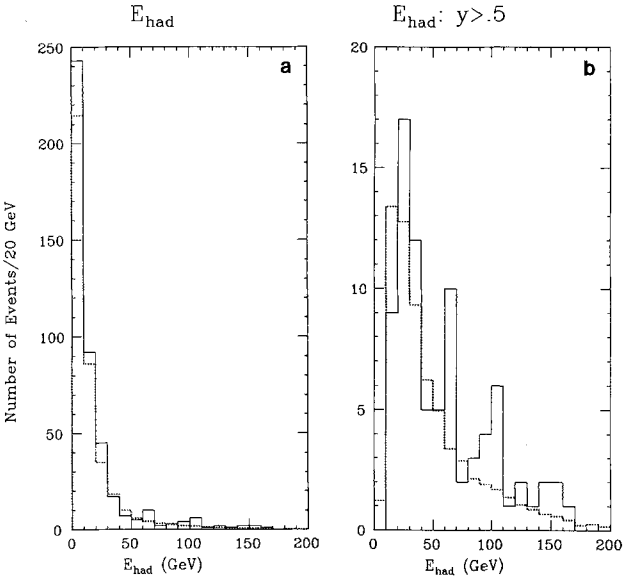

Fig. 7a, b

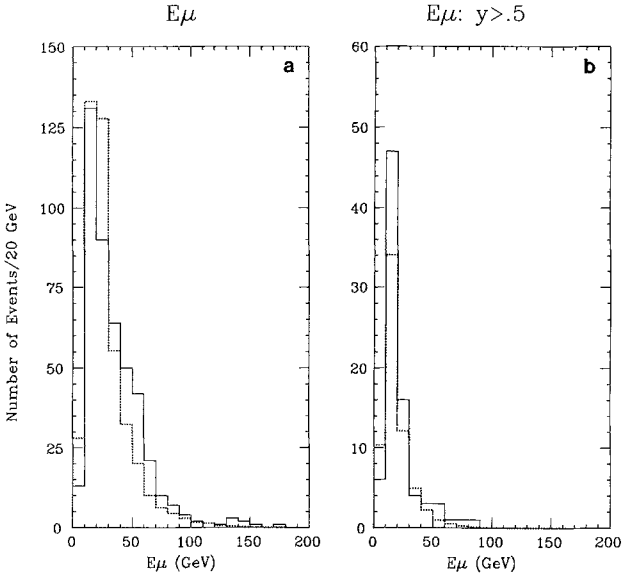

Fig. 6a, b

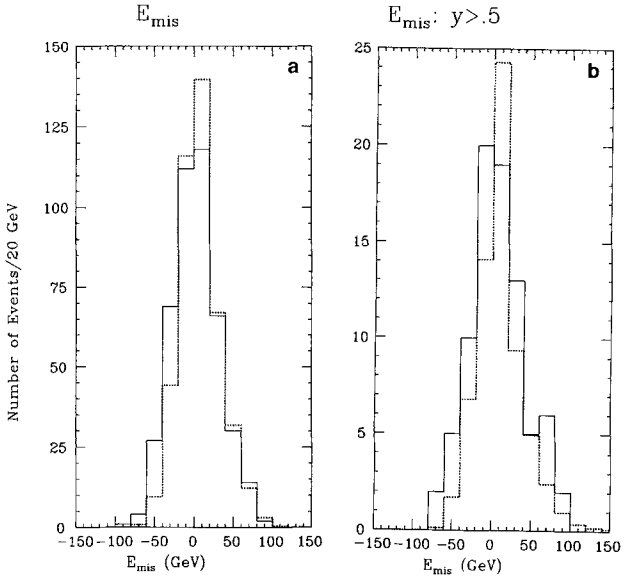

Fig. 8a, b

Fig. 5–8. Distribution of E_{vis}, E_{μ^+}, E_{had} and E_{mis} are presented for WSM data (solid line) and background (dotted line) in **5a**, **6a**, **7a** and **8a** respectively. Corresponding distributions for the case $y = y_{\text{vis}} = E_{\text{had}}/E_{\text{vis}} > 0.5$, are shown in **5b–8b**

dent neutrino E_ν is determined, within 10%, from the transverse vertex position at the detector [11]. The missing energy associated with an event is defined as $E_{\text{mis}} = E_\nu - E_{\text{vis}}$ and E_{mis}. E_{mis} distributions for the WSM sample are shown in Fig. 8. Since NC interactions, with μ^+ produced at the hadron vertex, constitute a background for WSM, there is missing energy (due to final state ν_μ) associated with these events. Figure 8b confirms this expectation. Table 1a lists mean kinematic quantities of WSM events and compares them with the background calculations discussed below. Quantities Q^2_{vis} and x_{vis} are defined as, $Q^2_{\text{vis}} = 2E_{\text{vis}} E_{\mu^+}(1-\cos\theta_{\mu^+})$ and $x_{\text{vis}} = Q^2_{\text{vis}}/(2M_N E_{\text{had}})$, respectively. Table 1b compares the same quantities for the WSM sample for events with $y > 0.5$ and $E_{\text{vis}} > 100$ GeV.

Charged current data were made to pass through the same set of cuts as the WSM data, with the exception that the muon was required to be focused in the spectrometer. The set of CC surviving all cuts consisted of 167000 events. Table 2 contains the means of the kinematic quantities associated with the CC sample. This set of CC events was used to normalize the ν_μ-induced background calculations. Normal-

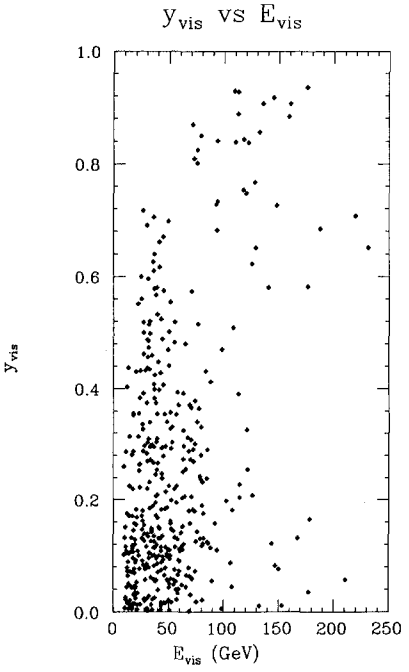

Fig. 9. y_{vis} vs E_{vis} for WSM data. The two bands in the above suggests the production of WSM at low-y, low-E_{vis} due to WBB $\bar{\nu}_\mu$ and at high-y, high-E_{vis} due to dileptons

Table 1a. Means of kinematic distributions of WSM data and backgrounds. All energies are in GeV. Q^2 is in $(GeV/c)^2$

Quantity	Data	WBB	Dilepton	WBB+ Dilepton
E_{vis}	53.3 ±1.7	39.4 ±2.0	104.3 ±1.9	42.0 ±2.0
$E_{\mu+}$	35.7 ±1.2	25.5 ±0.9	19.9 ±0.4	25.2 ±0.9
E_{had}	17.6 ±1.3	14.8 ±0.3	76.0 ±1.4	17.7 ±0.4
E_{mis}	1.5	19.9 ±2.0	7.8 ±1.6	
y	0.27±0.01	0.35±0.02	0.66±0.2	0.37±0.02
Q^2_{vis}	4.0±0.3	5.2±0.5	6.9±1.1	5.1±0.6
x_{vis}	0.23±0.01	0.24±0.02	0.11±0.02	0.24±0.02

Table 1b. Means of kinematic distributions of WSM data and backgrounds with $y>0.5$ and $E_{vis}>100$ GeV

Quantity	Data	WBB	Dilepton	WBB+ Dilepton
E_{vis}	143.2 ±6.8	125.4 ±6.4	145.4 ±2.6	140.1 ±2.6
$E_{\mu+}$	32.8 ±4.4	35.5 ±1.3	23.7 ±0.5	26.9 ±0.6
E_{had}	110.4 ±5.4	90.0 ±1.9	119.0 ±2.2	111.4 ±2.2
E_{mis}	23.9 ±8.0	15.6 ±1.2	24.4 ±2.5	22.2 ±2.4
y	0.78±0.03	0.72±0.04	0.83±0.03	0.80±0.03
Q^2_{vis}	12.5 ±0.9	23.6 ±2.3	5.9 ±0.9	10.2 ±1.0
x_{vis}	0.06±0.02	0.14±0.01	0.09±0.02	0.10±0.02

Table 2. Means of kinematic distributions of CC. The errors on the means of distributions are less than 1%

Quantity	CC-Data
E_{vis}	120.5
$E_{\mu-}$	67.0
E_{had}	53.5
E_{mis}	00.0
y	0.44
Q^2_{vis}	19.1
x_{vis}	0.21

Table 3. Normalization sample. Number of primary protons, secondary hadrons, fraction of K^+ in the secondary beam and the total CC-events in each energy setting of the secondary beam

Setting	Protons	Secondaries	K^+ Fraction	CC-Events
250 GeV	20.80×10^{17}	15.68×10^{15}	0.013	46240
200 GeV	11.55×10^{17}	8.05×10^{15}	0.027	40868
165 GeV	8.79×10^{17}	4.38×10^{15}	0.040	32375
140 GeV	8.14×10^{17}	3.54×10^{15}	0.045	29000
120 GeV	2.61×10^{17}	1.12×10^{15}	0.056	8623
100 GeV	3.59×10^{17}	1.00×10^{15}	0.065	9801

ization of the WBB background requires the total integrated primary proton flux on the target as well as the total intensity and the composition of the secondary mesons passing the beam-steering cuts. The intensity and the composition of the secondary beam are needed to compute the ν_e-induced WSM background (ν_e come from $K\to\pi+e^+\nu_e$ decays in the dichromatic train: see below). The number of primary protons on the target, the number of the secondary hadrons in the decay pipe, the fraction of K^+ in the secondary beam, and the corresponding number of $\nu_\mu-N$ CC-event for each of the six secondary beam settings are presented in Table 3.

Estimation of the known background sources of WSM

Pions and kaons that decay before momentum and sign selection in the dichromatic train constitute a source of diffused, low energy ν and $\bar{\nu}$ WBB. The modeling of this background is difficult since its production depends upon the various beam elements and the details of beam dumping. Any scraping of the beam along the pipe wall or along any collimator or insert along the beam line could be a potential source of the WBB. Therefore we have chosen to model this background by Monte Carlo techniques with direct checks against actual *background measure-*

Table 4. Sources of WBB $\bar{\nu}_\mu$-induced WSM with E_{vis} cut, shown as $\mathscr{E}$ (in GeV) in the table below, and with y cut

Source	$\mathscr{E}<100$	$\mathscr{E}>100$	$\mathscr{E}<100$ $y>0.5$	$\mathscr{E}>100$ $y>0.5$
Primary target	334.7	14.1	36.0	3.0
Primary dump	81.2	1.8	7.6	0.4
Decay pipe	6.8	0.2	0.0	0.0
Secondary dump	0.7	<0.1	0.0	0.0
μ^+-decay	0.1	<0.1	0.0	0.0

ments. The two major sources of WBB $\bar{\nu}_\mu$ are production and decay of π^-/K^- at (1) the primary BeO target and (2) the primary dump (where the uninteracted primary protons are deposited). Other sources include, (3) interaction of the secondary beam with material inside the decay pipe (Cerenkov counter, ionization chamber, etc.), (4) interaction of the secondary beam with the secondary dump at the end of the decay pipe, and (5) muon decays before ranging out in the earth shield. An outline of the WBB simulation has been given in Appendix A. Table 4 lists the contribution of various WBB sources to the WSM sample. The first two sources (see Table 4) required the total number of primary protons for normalization; the last three required measurements of the secondary beam intensity as well as its composition.

The simulation of WBB $\bar{\nu}_\mu$ was checked against data that were recorded with the momentum-defining slit at the end of the dichromatic magnet train closed (see Fig. 2). The data so accumulated, called the closed slit data, were subjected to the WSM cuts discussed above. The resulting sample, when scaled by the ratio of proton intensity during the normal running (open slit) to that of the closed slit running (ratio = 19.7), provided a direct measure of the WBB component of the WSM (see Table 5a and b). When scaled the closed slit data yield 375.1 ± 85.9 WBB $\bar{\nu}_\mu$ events, with $E_{vis}<100$ GeV, contributing to the WSM sample – to be compared with the corresponding WBB MC prediction of 433.9 ± 86.4 events. The error in the MC estimation represents the systematic uncertainty in the WBB modeling as outlined in Appendix A. The agreement between data and Monte Carlo lends credence to the WBB MC calculation, particularly when extrapolated to $E_{vis}>100$ GeV region where there is unsufficient closed slit data.

Another source of WSM is the production of dileptons ($\mu^-\mu^+, e^-\mu^+$ or $\nu_\mu\mu^+$) where the lepton at the neutrino vertex, called the leading lepton (μ^-, e^- or ν_μ) is unobserved. ν_μ-induced opposite-sign dimuons (OSDM) arise from the CC production of charm and its subsequent muonic decay: $\nu_\mu + d(s) \to \mu^- + c + X$, where c-quark fragments into a charmed hadron, D, which then semileptonically decays into a μ^+. There are two ways in which the leading muon might evade detection: it could exit the sides of the detector, or it could range out in the target and be lost in the hadron shower. This background was modeled with OSDM events generated using a dimuon Monte Carlo [1]. The penetration of the hadron shower was simulated using data accumulated during a test run in May-June 1984 at Lab E [12]. In order to be observed, the leading muon (μ^-) must have penetrated at least three spark chambers (≈ 60 cm of steel) beyond the end of the hadron shower. The candidate $\mu^-\mu^+$ events were subjected to WSM cuts and were normalized to the CC sample. The total contribution of this background to the WSM sample was 8.2 events of which 3.6 events had $y>0.5$ and $E_{vis}>100$ GeV. Figure 10 shows the E_{vis} spectrum of WSM coming from this source (solid line) and Tables 5a and b collate this background with the data with and without the y cut.

Incident ν_e from K^+ decay in the decay pipe can also produce an apparent WSM signal. The flux of ν_e has been illustrated in Fig. 3. A dilepton induced by a ν_e could give rise to a WSM as follows: $\nu_e + d(s) \to e^- + c + X$, where c-quark fragments into a charmed hadron, D, which then semileptonically de-

Table 5a. WSM. Data vs background without the y cut closed slit data, normalized background estimates and WSM data

WSM type	$E_{vis}<100$ GeV	$E_{vis}>100$ GeV
Scaled closed slit data	375.1 ± 85.9	0 ± 19.7
WBB MC	423.5 ± 85.4	16.2 ± 3.0
$\mu^-\mu^+$ MC	4.1 ± 0.9	4.1 ± 0.9
ν_e-induced μ^+ MC	2.4 ± 0.4	3.0 ± 0.6
NC-induced π^+/K^+ decay MC	3.9 ± 0.8	3.6 ± 0.8
Total background MC	433.9 ± 86.4	26.9 ± 5.1
WSM data	400 ± 20	43 ± 6.6

Table 5b. WSM. Data vs background with $y>0.5$

WSM type	$E_{vis}<100$ GeV	$E_{vis}>100$ GeV
Scaled closed slit data	19.7 ± 19.7	0 ± 19.7
WBB MC	43.6 ± 8.5	3.4 ± 0.6
$\mu^-\mu^+$ MC	3.6 ± 0.8	3.6 ± 0.8
ν_e-induced μ^+ MC	2.4 ± 0.4	3.0 ± 0.6
NC-induced π^+/K^+ decy MC	3.4 ± 0.6	3.6 ± 0.7
Total background MC	53.0 ± 10.5	13.6 ± 2.7
WSM data	58 ± 7.6	24 ± 4.9

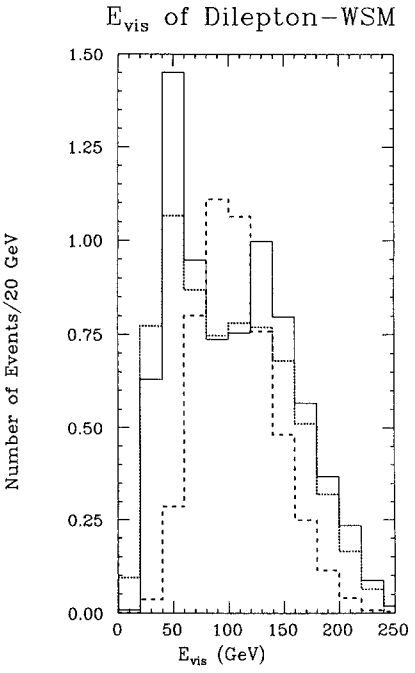

Fig. 10. Simulation of E_{vis} spectrum of the three dilepton induced WSM: $\mu^-\mu^+$ where the μ^- remains undetected (solid line), ν_e-induced $e^-\mu^+$ (dashed line) and NC production and decay of π^+/K^+ into an isolated μ^+

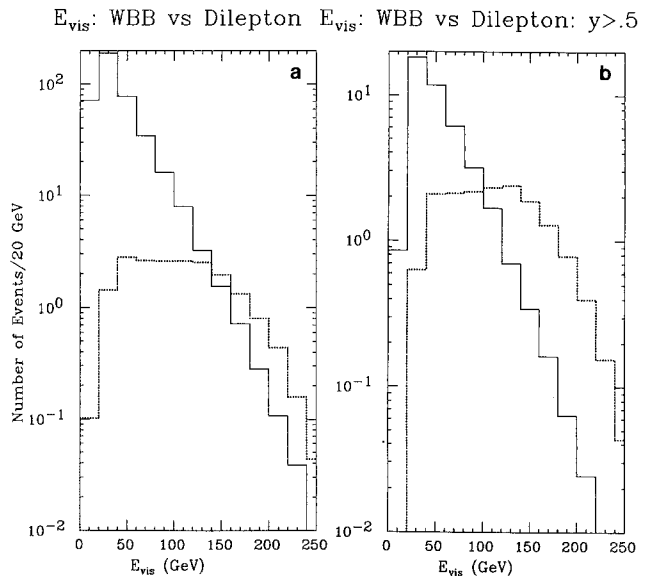

Fig. 11. a A simulation of E_{vis} spectrum for WBB (solid line) and dilepton (dotted line) induced WSM without any cut on y. **b** the same comparison for $y>0.5$. For $E_{vis}>100$ GeV the dilepton background dominates the WBB

cays into a μ^+. In our detector an electron would appear as hadron shower, and, consequently its energy was added to the hadron shower energy. To compute this background, the spectrum of the electron neutrino at the detector was calculated from the kaon content of the secondary beam. This flux was then used to generate CC events, which in turn were employed to simulate the production of c-quarks and their semileptonic decay into a μ^+. The calculation yielded 5.4 WSM events, 3.0 of which had $y>0.5$ and $E_{vis}>100$ GeV. Figure 10 displays the WSM events from this source (dashed line) and Table 5a, b list these along with other backgrounds.

In an NC interaction a μ^+ could result from the production and subsequent decay of π^+/K^+ in the hadron shower. This WSM background is analogous to the background for the opposite-sign dimuons from the hadron shower and is estimated using a Monte Carlo program similar to that discussed in [1]. We calculated 7.5 WSM events generated via this mechanism, of which 3.6 events had $y>0.5$ and $E_{vis}>100$ GeV. The energy spectrum of WSM from this source (after the standard cuts) is displayed in Fig. 10 (dotted line). The comparison of this background with others is carried out in Table 5a, b.

Figure 11a contrasts the contribution of the WBB with the dilepton background. WBB dominates the dilepton background. However, after requiring the cut $y>0.5$ (see Fig. 11b) and $E_{vis}>100$ GeV, the dominant background is the latter. The characteristic kinematic quantities for the backgrounds are given in Table 1a, b.

Finally, cosmic rays (CR) constitute a small background for WSM at low energy. A sample of cosmic ray events was accumulated during regular running. The sample when subjected to the standard WSM cuts and scaled according to the fraction of the time the detector was live (treating the open and closed slit data separately) provided a measurement of the CR background. The CR background did not survive the $y>0.5$ cut, and no CR event had an energy above 100 GeV.

Results and discussion

Table 6 summarizes the observed WSM data and the computed cumulative background with no y cut, with $y>0.5$ and with $y<0.5$ for $E_{vis}<100$ GeV and $E_{vis}>100$ GeV. The error associated with the background computation is estimated to be $\approx 20\%$ (see [1] and Appendix A). For $E_{vis}<100$ GeV, all of the WSM events are accounted for as background, most are due to the WBB $\bar{\nu}_\mu$. Consequently, we consider only events with E_{vis} greater than 100 GeV. There is an excess of 16.1 ± 8.3 events; the corresponding excess with $y>0.5$ is 10.4 ± 5.6. The validity of the background calculation and estimate of the systematic uncertainties have been investigated in the data with several cross-checks. The background estimate of the low energy WSM agrees well with the observed

Table 6. Summary of WSM analysis. WSM events with E_{vis} cut, shown as $\mathscr{E}$ (in GeV) in the table below, and with y cut. Quantities in the adjacent lines, preceded by $\pm$, represent errors

Category	$\mathscr{E}<100$	$\mathscr{E}>100$	$\mathscr{E}<100$ $y>0.5$	$\mathscr{E}>100$ $y>0.5$	$\mathscr{E}<100$ $y<0.5$	$\mathscr{E}>100$ $y<0.5$
Data	400	43	58	24	342	19
	($\pm$20)	($\pm$6.6)	($\pm$7.6)	($\pm$4.9)	($\pm$19)	($\pm$4.4)
Background	433.9	26.9	53.0	13.6	380.9	13.3
	($\pm$86.4)	($\pm$5.1)	($\pm$10.5)	($\pm$2.7)	($\pm$84.9)	($\pm$3.2)
Excess		16.1		10.4		5.7
		($\pm$8.3)		($\pm$5.6)		($\pm$5.4)

closed slit data. The extrapolation of the WBB MC to $E_{vis}>100$ GeV raises the question: could something cause the high energy WBB $\bar{\nu}_\mu$ to increase without appreciably affecting its low energy content? Presence of holes in the dump, for example, could bring about such an effect. However, above 100 GeV the contribution to the calculated WSM sample from the primary dump is ≈ 1.5 events; even if this contribution were doubled, the significance of the excess WSM remains essentially unchanged. The y cut offers further insight into the WBB component of the WSM sample. Above 100 GeV, the WBB MC predicts 3.4 events in the data. If one were to assume the entire WSM sample of 43 events with $E_{vis}>100$ GeV are due to WBB and accordingly increase the WBB component for the case $y>0.5$ from 3.4 events to 6.8 events, the excess WSM is 7.0 ± 5.3 events. The significance of the excess decreases from 1.9σ to 1.3σ. Finally, the data and the background do not display any kinematic disparity. The above consideration suggests that there is no compelling signal for prompt WSM's.

Using these data to set upper limits on the rate of WSM production requires correction for the acceptance of the apparatus. This acceptance correction requires that the production mechanism of excess WSM be known. Assuming the excess WSM to have a similar kinematic distribution to the background, we estimate the acceptance from MC calculation. For $y>0.5$, the three dilepton backgrounds yield similar acceptance corrections and the average acceptance corrected rate for prompt WSM was $(1.6\pm0.9)\times10^{-4}$ per CC event. The corresponding rate for the case $y<0.5$ (assuming that the excess has kinematic properties like $\bar{\nu}_\mu$) was $(6.4\pm6.1)\times10^{-5}$ per CC event. The corresponding 90% upper confidence limits on the WSM production are 3.1×10^{-4} and 1.6×10^{-4} per CC event for the cuts $y>0.5$ and $y<0.5$ respectively.

The upper limit on the production of WSM events places a limit on the charmed component of the nucleon sea. This process is shown in Fig. 1a. The charmed sea of the nucleon, characterized by low-x, should be distinguished from the intrinsic charm of the nucleon [13] where $x\to1$ and the nucleon comprises five 'valance quarks', i.e. $|uudc\bar{c}\rangle$. Intrinsic charm is severely constrained by the Fermilab experiment E 595 [14]. WSM data help constrain the charmed sea. The upper limit on the charmed component of the nucleon is found by taking the ratio of the WSM to OSDM and comparing this ratio to the theoretical prediction. The steps in computing the charmed sea are outlined in Appendix B. Let

$$\xi=x+\xi_{\min}=\frac{Q^2}{2M_N\nu}+\frac{m_c^2}{2M_N\nu}$$

be the fractional momentum carried by the c-quark, where ν represents the energy transfer to hadrons and $\xi_{\min}$ represents the threshold fractional momentum for a heavy quark. For an isoscalar target, if

$$\eta_c=\frac{2C}{U+D}\text{ where,}$$

$$C=\int_{\xi_{\min}}^{1}\xi c(\xi)\,d\xi,\quad\text{and,}$$

$$(U+D)=\int_0^1 x(u(x)+d(x))\,dx,$$

then it is found that

$$\eta_c<0.035\,(90\%\text{ CL}).$$

Wrong sign muons would also be produced by flavor changing neutral current (FCNC) transitions of u-quarks to c-quarks (Fig. 1b). Using the above WSM limits we calculate limits on the relative rate of FCNC:

$$\frac{\sigma(\text{FCNC})}{\sigma(\text{NC})}=\frac{\#\text{ of WSM events}}{\#\text{ of NC events}}\times\left(\left[\int_0^1 D_c^p(z)\,dz\right]\times[\text{Br}(D\to\mu^+\nu_\mu+X)]\right)^{-1},$$

Table 7. "Neutral current analog" (e.g. FCNC) of OSDM and WSM. Events with $E_{vis} > 100$ GeV, and for the last two columns with an additional $y > 0.5$ were considered for this comparison

Quantities	OSDM data	'NC analog' of OSDM	WSM data
# of Events	163 ±12.8	67 ±8.2	20 ±4.5
Background	11 ± 2.2	5.2 ±1.0	8.5 ±1.7
Excess	152 ±12.9	61.8 ±8.3	11.5 ±4.8
E_{vis}	150.7 ± 3.7	136.0 ±3.2	148.8 ±7.8
Lead E_μ	61.9 ± 2.8		
Non lead E_μ	23.8 ± 1.1	25.8 ±1.7	35.3 ±4.9
E_{had}	64.6 ± 2.7	109.2 ±3.5	113.5 ±6.2
E_{mis}	8.8 ± 1.9	22.8 ±3.1	20.1 ±9.5
y	0.42± 0.01	0.80±0.01	0.77±0.03

where $D_c^D(z)$ represents the c-quark fragmentation into a charmed hadron with a fractional momentum z and the last term signifies the semileptonic decay of the D-meson. The limit is:

$$\frac{\sigma(\text{FCNC})}{\sigma(\text{NC})} < 8.5 \times 10^{-3} \text{ (90\% CL)}.$$

CDHS has extracted a corresponding limit of 2.6×10^{-2} (90% CL) [15].

If FCNC were responsible for WSM production via u- to c-transition (Fig. 1b), then WSM may constitute the NC analog of the mechanism which produces OSDM in CC interaction. In order to investigate this, the OSDM, WSM and CC data samples were extracted using identical cuts. The relevant backgrounds were calculated for each of the new samples. The leading muon [1] of the OSDM was treated as if it were unobserved (i.e., as a neutrino) and the μ^+ of WSM was assumed to originate at the hadron vertex. Table 7 presents the comparison of the WSM and OSDM samples. Events with $y > 0.5$ and $E_{vis} > 100$ GeV were considered for this comparison. The table shows the number of events, backgrounds and means of kinematic distributions. Kinematic variables such as the E_{had}, y, and E_{mis} are similar for the two classes of events. However, the paucity of WSM events hinders the drawing of quantitative conclusions about a deeper connection between the two.

If WSM events were brought about by a lepton number violating interaction, then the upper limit on the WSM production rate relative to the CC for the case $y < 0.5$ is:

$$\frac{\sigma(\nu_\mu - \text{induced lepton number violating interaction})}{\sigma(\text{CC})} < 1.6 \times 10^{-4}$$

at 90% CL. If the oscillation of ν_μ to $\bar{\nu}_\mu$ were responsible for WSM production, then the above upper limit constrains the oscillation parameter, $\Delta m^2 \sin 2\alpha$ where $\Delta m^2 = |m_1^2 - m_2^2|$, as follows: the fraction of $\bar{\nu}_\mu$ in a ν_μ beam at a distance L from the origin of ν_μ is given by [16],

$$\mathcal{R} = \frac{1}{2}\left(1 - \cos\frac{2\pi L}{\mathcal{L}}\right)\sin^2 2\alpha$$

where $\mathcal{L} = 4\pi E_\nu hc/\Delta m^2$ is the characteristic oscillation length. For our $y < 0.5$ & $E_{vis} > 100$ GeV WSM sample $E_\nu = 143$ GeV and $L = 1116$ m. Using the above upper limit on WSM production and assuming $\mathcal{L} \gg L$ we obtain:

$\Delta m^2 \sin 2\alpha < 1.3$ eV^2 (90% CL).

It has been suggested that a massless Majorana neutrino might mediate neutrinoless double beta decay [17]. Such a neutrino will produce WSM's. If we further assume that a massless Majorana neutrino with right-handed coupling is causing this violation, the above upper limit can be used to derive a limit on the mass and the mixing angle of the right-handed boson (W_R) mediating the right-handed coupling. If we assume the physical gauge bosons mediating the weak interaction to be admixtures of the left and the right-handed gauge bosons, i.e.,

$$W_1 = W_L \cos\zeta + W_R \sin\zeta,$$
$$W_2 = -W_L \sin\zeta + W_R \cos\zeta,$$

where ζ is the mixing angle, the previous limit leads to the limits $M_{W_R} < 8.89 \times M_{W_L} = 729$ GeV if $\zeta = 0$ and $\zeta < 0.72°$ if $M_{W_R} \to \infty$.

Conclusion

Our analysis indicates that there is no signal for prompt WSM events. The absence of a definite like-sign dimuon event signal at the Tevatron [4] rules out the possibility of exotic sources giving rise to LSDM, and, in our opinion, to WSM as well. The excess observed here indicates that WSM could be a low energy phenomenon, quite similar to the LSDM excess observed in low energy experiments. Whether or not this supposition is valid, the upper limit on the WSM rate does offer an opportunity to set limits on various exotic processes.

Acknowledgements. We are grateful for the gracious hospitality of the Fermilab staff and for the dedicated efforts of many individuals at our home institutions. This research was supported by grants from the National Science Foundation and the U.S. Department of Energy.

Appendix A: ν_μ wide band background calculation

The principal source of background for WSM events is WBB $\bar{\nu}_\mu$-induced CC events. The prominent source of $\bar{\nu}_\mu$ is production and subsequent decay of π^-/K^- at the primary target and primary dump. The estima-

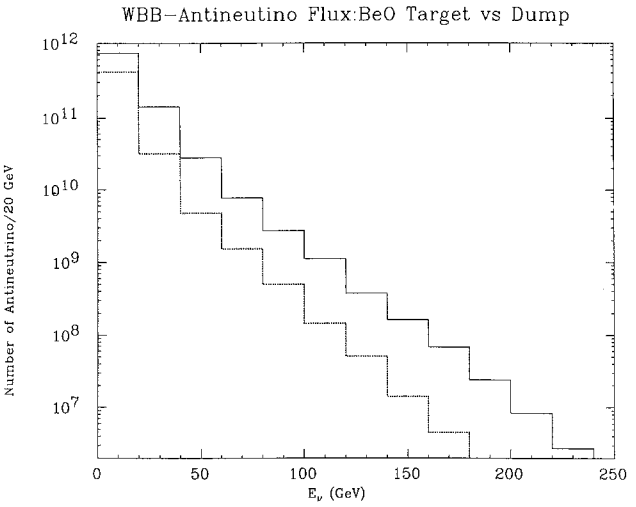

Fig. 12. WBB $\bar{\nu}_\mu$ flux at Lab$-E$ originating at the primary target (solid line) versus those that originate at the primary dump (dotted line). The above simulation suggests that the the dominant WBB component (with $E_{\text{vis}} > 100$ GeV) is the interaction of primary protons at the BeO target

tion of the contribution of this background to WSM involved the determination of the antineutrino flux, followed by the convolution of this flux with the detector acceptance for $\bar{\nu}_\mu$-induced events.

The calculation of WBB $\bar{\nu}_\mu$ originating at the primary target used a model of production of secondary particles such as, π^+, π^-, K^+ and K^-, by the 400 GeV protons from the measurement by Atherton et al. [18]. The secondary particles were traced through the beam elements with the aid of the Turtle program [19]. Most of the negative secondary particles (mostly π^- and K^-) were focused out of the beam by the time they reached the third beam element (2.1 m from the BeO target). A weight was assigned to each π^-/K^- quantifying the probability of its decay during the flight. Finally the detector acceptance was folded in to arrive at the WBB $\bar{\nu}_\mu$ flux at our detector. The flux was normalized to the total proton flux.

The calculation of WBB $\bar{\nu}_\mu$ originating at the primary dump was concerned with an Al-insert in the dichromatic beam line that absorbed, principally, the 400 GeV protons which did not interact in the primary target. The position of the dump and the angle of dumping varied from energy setting to energy setting. The details of the dump calculation followed [20], [21]; and was cross-checked against the CERN beam experiment results [22, 23]. The WBB $\bar{\nu}_\mu$ flux at our detector from the two sources is shown in Fig. 12. The cumulative proton flux for the two runs was 5.55×10^{18}. The figure illustrates that the WBB $\bar{\nu}_\mu$ flux from the BeO target is a factor of three higher than that from the dump at energy below 100 GeV. Above 100 GeV the contribution of the dump is lower by an order of magnitude.

There are three other less significant surces of WBB $\bar{\nu}_\mu$ that contribute to the WSM background. The secondary particles in the decay region, consisting of π^+, K^+ and protons, could interact with the material of the flux monitoring devices. The total material in the decay pipe was estimated to be 0.077 of an interaction length. Another source of the WBB $\bar{\nu}_\mu$ background is the secondary dump which is meant to absorb the hadrons emerging from the decay region. However, hadrons interacting in the secondary dump are typically at half the energy and four orders of magnitude lower intensity than those interacting in the primary dump. Flux from this source was estimated and included in the overall background. Finally, μ^+ originating from π^+/K^+ decays can themselves decay between the decay region and the earth shield and produce $\bar{\nu}_\mu$. However, the small number of π^+/K^+ decays (3% to 4% of the π^+/K^+ decay), low energy of the muons and their long life time and the small solid angle subtended by the detector (the detector was located 940 m away from the downstream end of the decay pipe) made this an insignificant background. The flux from all these sources was convoluted with the detector acceptance for a $\bar{\nu}_\mu$-induced CC event.

The systematic error in estimating the WBB component of WSM occur in the following three stages: a) Production of the secondary mesons, π^-/K^-, from primary protons. The systematic uncertainty in the measurements of Atherton et al. [15] contributes 8% error. The data with $P_T \approx 300$ MeV, however, have an additional uncertainty of 6%. We estimate the overall error from the production uncertainty to be 10%. b) Error in simulating the hadron beam. The errors in Turtle calculation [19] have been discussed in detail, and, for our calculation, is estimated to be 10%–15%. This estimate, it should be noted, includes the proton spot-size on the target. In addition to the above, the dump-calculation has larger errors ($\approx 50\%$) due to uncertainty in the details of beam dumping. c) Error in simulating the $\bar{\nu}_\mu$-interactions in the detector. The critical factor here is the precision to which the antiquark distributions are known. The cumulative error due to this and apparatus acceptance etc. is estimated at 8%–9%.

The overall error in computing wrong-sing WBB contribution to our sample of WSM is estimated to be 20%. Table 4 presents the contribution of all these WBB $\bar{\nu}_\mu$ sources to the WSM sample.

Appendix B: charmed content of the nucleon sea

The upper limit on WSM rate offers a means to set a limit on the charmed content of the nucleon sea.

The differential cross-section of the neutral current scattering of a neutrino by a charm quark is given by,

$$\frac{d\sigma}{d\xi\, dy}=\frac{G_F^2 M_N E_\nu}{\pi}$$
$$\cdot\left(|g_L^c|^2+|g_R^e|^2(1-y)^2-\frac{1}{2}(\bar{g}_L^c g_R^c+\bar{g}_R^c g_L^c)\frac{M_N}{E_\nu}\right)\xi c(\xi)$$

where $g_L^c=t_3^c-Q_c^2\sin^2\theta_W$, $g_R^c=-Q_c^2\sin\theta_W$, the scaling variable $\xi=\frac{Q^2+m_c^2}{2M_N\nu}$ signifies the fractional momentum of the charm quark with a distribution given by $c(\xi)$. Using $t_3^c=1/2$, $Q_c=2/3$ and our mesured value of $\sin^2\theta_W$ [24]; and integrating over the variables y and ξ, one gets:

$$\sigma(\nu_\mu+c\to\nu_\mu+c)=\frac{G_F^2 M_N E_\nu}{\pi}(0.127)\,C$$

where the term proportional to M_N/E_ν has been neglected and the total momentum carried by the charm quark, C, is given by:

$$C=\int_{\xi_{\min}}^{1}\xi c(\xi)\,d\xi.$$

The struck charm quark then fragments into a D-meson, which semileptonically decays into a μ^+. Thus the cross-section for production of a WSM from a c-quark is given by:

$$\sigma(\nu_\mu+N\to\mu^++X)=\sigma(\nu_\mu+c\to\nu_\mu+c)\times\left(\int_0^1 D_c^D(z)\,dz\right)$$
$$\times(\mathrm{Br}\,(D\to\mu^++\nu_\mu+X)).$$

The cross-section for producing a prompt charmed opposite-sign dimuon in $\nu_\mu-N$ scattering is identical to the above except for the first term. Therefore, to the first order, the ratio of cross-sections for the two processes could be written as:

$$\frac{\sigma(\nu_\mu+N\to\mu^++X)}{\sigma(\nu_\mu+N\to\mu^-+\mu^++X)}$$
$$=0.127\frac{2C}{(U+D)\sin^2\theta_c+2S\cos^2\theta_c}$$

where $(U+D)=\int_0^1 x[u(x)+d(x)]\,dx$, $S=\int_0^1 xs(x)$ and θ_c is the Cabbibo angle. The strange quark content of the nucleon, expressed as η_s, has been measured [1] to be, $\eta_s=\frac{2S}{(U+D)}=0.075\pm0.019$ for $E_\nu>100$ GeV. We express the charm content of the nucleon sea analogously as:

$$\eta_c=\frac{2C}{(U+D)}.$$

Using the upper limit on the acceptance corrected WSM rate and the rate of prompt OSDM production, we arrive at an upper limit on η_c:

$$\eta_c<0.035\,(90\%\ \mathrm{CL}).$$

References

1. K. Lang et al.: Z. Phys. C – Particle and Fields 33 (1987) 483 and references therein
2. M. Veltman: UM 83-22 (1983), Univ. of Michigan Preprint
3. D. Schildknecht in: XIX Rencontre de Moriond, La Plagne, 1984
4. B.A. Schumm et al.: Phys. Rev. Lett. 60 (1988) 1618
5. V. Berger et al.: Nucl. Phys. B123 (1977) 132
6. D.A. Edwards, F.J. Sciulli: Fermilab Preprint T.M.-660, 2972.000
7. R.E. Blair et al.: Nucl. Instrum. Methods, 226 (1984) 281
8. G. Fisk, F.J. Sciulli: Ann. Rev. Part. Sci. 32 (1982) 499
9. D. MacFarlane et al.: Z. Phys. C – Particle and Fields 26 (1984) 1
10. The direction of the secondary beam was monitored by the split-plate ionization chambers. For details see [7]
11. Events due to ν_π and ν_K were distinguished by comparing the energy expected from the transverse radial position of the interaction and measured total energy. Once this separation was made the transverse radius at the detector and the mean energy of the secondary meson determined the incident neutrino energy
12. F.S. Merritt et al.: Nucl. Instrum. Methods A245 (1986) 27
13. S. Brodsky et al.: Phys. Lett. 93B (1980) 451; Phys. Rev. D23 (1981) 2745
14. A. Bodek et al.: Phys. Lett. 113B (1982) 77
15. M. Holder et al.: Phys. Lett. 74B (1978) 277
16. I.E. Stockdale et al.: Phys. Rev. Lett. 52 (1984) 1384; Z. Phys. C – Particles and Fields 27 (1985) 53
17. M. Shaevitz, in: Proceedings of 1983 International Symposium on Lepton and Photon Interactions at High Energies, D.G. Cassell, D.L. Kreinick (eds.) 1983, p 132
18. H.W. Atherton et al.: CERN 80-07, 22 1980. A separate parametrization of the Atherton et al. data has been put forward by A.J. Malensek: FNAL Technical Memo, FN-341, 2941, 000
19. D. Carey: Turtle, Fermilab Preprint NAL-64, 2041.000
20. S. Mori: Estimated event rates for beam dump experiments. FNAL TM-774, 2251.000, 1978; and also: Estimated ν_τ flux from a beam dump at 400 GeV and 1000 GeV. FNAL TM-848, 2251.000, 1979
21. C.H. Albright et al.: Signal for ν_t events in a beam dump experiment. Fermilab-conf-79/36-THY, 1979
22. H. Abramowicz et al.: Prompt neutrino production in proton beam dump experiment. CERN-EP/82-17, 1982
23. H. Wachsmuth: Neutrino and Muon fluxes in the CERN 400 GeV proton beam dump experiment. CERN-EP/79–125, 1979
24. P. Reutens et al.: Phys. Lett. 152B (1985) 404